The Astrophysical Journal, 637:138–146, 2006 January 20

LINER-LIKE EXTENDED NEBULAE IN ULIRGs: SHOCKS GENERATED BY MERGER-INDUCED FLOWS

A. Monreal-Ibero[1]
Instituto de Astrofísica de Canarias, c/ Vía Láctea s/n, 38200 La Laguna, Tenerife, Spain; amonreal@aip.de
S. Arribas[2,3]
Space Telescope Science Institute, 3700 San Martin Drive, Baltimore, MD 21218; arribas@stsci.edu
and
L. Colina
Instituto de Estructura de la Materia, Consejo Superior de Investigaciones Científicas (CSIC),
Serrano 121, 28006 Madrid, Spain; colina@isis.iem.csic.es
Received 2005 July 13; accepted 2005 September 21

ABSTRACT

In this work we studied the two-dimensional ionization structure of the circumnuclear and extranuclear regions in a sample of six low-z ultraluminous infrared galaxies using integral field spectroscopy. The ionization conditions in the extranuclear regions of these galaxies (∼5–15 kpc) are typical of LINERs as obtained from the Veilleux-Osterbrock line ratio diagnostic diagrams. The range of observed line ratios is best explained by the presence of fast shocks with velocities of 150–500 km s^{-1}, while ionization by an AGN or nuclear starburst is in general less likely. The comparison of the two-dimensional ionization level and velocity dispersion in the extranuclear regions of these galaxies shows a positive correlation, further supporting the idea that shocks are indeed the main cause of ionization. The origin of these shocks is also investigated. Despite the likely presence of superwinds in the circumnuclear regions of these systems, no evidence for signatures of superwinds such as double velocity components is found in the extended extranuclear regions. We consider a more likely explanation for the presence of shocks, the existence of tidally induced large-scale gas flows caused by the merging process itself, as evidenced by the observed velocity fields characterized by peak-to-peak velocities of 400 km s^{-1} and velocity dispersions of up to 200 km s^{-1}.

Subject headings: galaxies: active — galaxies: interactions — galaxies: nuclei — galaxies: starburst

Online material: color figures

1. INTRODUCTION

Ultraluminous infrared galaxies (ULIRGs), defined as objects with an infrared luminosity similar to that of optically selected quasars ($L_{\rm bol} \approx L_{\rm IR} \gtrsim 10^{12}\ L_{\odot}$), may be the local counterpart of some high-z galaxy populations (see Sanders & Mirabel 1996; Genzel & Cesarsky 2000; Frayer et al. 2003; Le Floc'h et al. 2004). Most (if not all) of them show signs of mergers and interactions (e.g., Clements et al. 1996; Scoville et al. 2000; Surace et al. 2000; Borne et al. 2000), and it has been found that they could be the progenitors of intermediate-mass elliptical galaxies (Genzel et al. 2001; Tacconi et al. 2002 and references therein). They have large amounts of gas and dust and are undergoing intense starburst activity. Some of these objects may harbor an active galactic nucleus (AGN), although its importance as a source of energy in ULIRGs is still under debate.

The origin of the ionization of gas in these objects has been mainly studied in the innermost (nuclear) regions (e.g., Kim & Sanders 1998). These studies show that ∼35% of their nuclei have a LINER-like ionization that is independent of the luminosity, while the fraction of the Seyfert-like spectrum increases with luminosity. However, due to the complex structure of the galaxies' central regions, studies based on nuclear optical spectroscopy may lead to misclassifications. This may have several causes. For instance, the actual nucleus of the system may be obscured in the optical, or alternatively, the dominant region in the emission line may not be coincident with the nucleus. An example for which both effects have been reported is IRAS 12112+0305 (Colina et al. 2000). In addition, standard slit spectroscopic observations may be affected by other types of technical uncertainties such as misalignment of the slit and differential atmospheric refraction.

ULIRGs, as systems that are undergoing an intense starburst activity phase (and with AGN activity in some cases), are good candidates to produce superwinds (see Veilleux et al. 2005). Evidence of superwinds has already been reported in several systems, on the basis of the properties of the emission (Heckman et al. 1990; Lehnert & Heckman 1996; Arribas et al. 2001) and absorption (Heckman et al. 2000; Rupke et al. 2002, 2005a, 2005b; Martin 2005) lines. Although superwinds are probably playing a role in the ionization of the circumnuclear region of ULIRGs, their importance in the extranuclear regions is unclear. In those regions, tidally induced forces associated with the interaction process itself have also been proposed as the mechanism responsible for shocks (McDowell et al. 2003; Colina et al. 2004).

The present article is focused on the study of the two-dimensional structure and mechanisms of ionization of six ULIRGs based on the use of integral field spectroscopy (IFS). This observational technique is well suited for this goal, since it allows us to simultaneously obtain spectral information of a two-dimensional field. The present work is part of a program aimed at studying the internal structure and kinematics of (U)LIRGs,

[1] Current address: Astrophysikalisches Institut Potsdam, An der Sternwarte 16, D 14482 Potsdam, Germany.
[2] On leave from the Instituto de Astrofísica de Canarias (CSIC).
[3] Affiliated with the Space Telescope Division of the European Space Agency, European Space Research and Technology Centre, Nordwijk, Netherlands.

TABLE 1
ULIRGs Sample

Galaxy	z	Scale (kpc arcsec^{-1})	$\log(L_{IR}/L_{\odot})$	f_{12}[a] (Jy)	f_{25}[a] (Jy)	f_{60}[a] (Jy)	f_{100}[a] (Jy)
IRAS 08572+3915	0.058[b]	1.20	12.15	0.32	1.70	7.43	4.59
IRAS 12112+0305	0.073[b]	1.52	12.30	0.11	0.51	8.50	9.98
IRAS 14348−1447	0.083[b]	1.72	12.31	0.14	0.49	6.87	7.07
IRAS 15206+3342	0.125[b]	2.60	12.18	0.08	0.35	1.77	1.89
IRAS 15250+3609	0.054[c]	1.12	12.03	0.20	1.32	7.29	5.91
IRAS 17208−0014	0.043[c]	0.89	12.40	0.19	1.66	3.11	3.49

[a] Vizier Online Data Catalog, 2156 (M. Moshir et al. 1993).
[b] Kim & Sanders (1998).
[c] Kim et al. (1995).

using this technique and high-resolution images obtained with the *Hubble Space Telescope* (*HST*; see Colina et al. 2005 and references therein). The paper is structured as follows: In § 2, we briefly describe the sample of galaxies analyzed and summarize how observations were performed. In § 3, the reduction process and data analysis are described. Section 4 presents the results obtained both in the external parts and in the nuclear regions and discusses the mechanisms responsible for the observed ionization. Section 5 summarizees the main conclusions.

Throughout the paper, a Hubble constant of 70 km s^{-1} Mpc^{-1} is assumed. This implies a linear scale between 0.89 and 2.58 kpc arcsec^{-1} for the systems analyzed.

2. SAMPLE AND OBSERVATIONS

2.1. *The Sample of Galaxies*

The sample of galaxies consists of six low-z ULIRGs (see general properties in Table 1) covering a relatively wide range of dynamical states of the merging process. Three of the galaxies (IRAS 08572+3915, IRAS 12112+0305, and IRAS 14348−1447) are interacting pairs separated by projected distances of up to 6 kpc, while the rest of the galaxies (IRAS 15206+3342, IRAS 15250+3609, and IRAS 17208−0014) are more evolved, single-nucleus ULIRGs, some with a light profile and overall kinematics close to that of intermediate-mass elliptical galaxies (e.g., IRAS 17208−0014; Genzel et al. 2001). The two-dimensional kinematic properties (velocity field and velocity dispersion) have been studied in detail previously using integral field optical spectroscopy (see Colina et al. 2005 and references therein).

The complexity of the two-dimensional ionization field in these galaxies is such that previous long-slit spectroscopic studies have classified the nucleus of several of the galaxies differently. For example, IRAS 08572+3915 was originally classified as Seyfert type 2 (Sanders et al. 1988), although both nuclei were classified as LINERs later on (Kim & Sanders 1998). IRAS 14348−1447 has been classified as either LINER (Kim & Sanders 1998) or Seyfert type 2 (Sanders et al. 1988), IRAS 15206+3342 has been identified both as a Seyfert type 2 (Sanders et al. 1988; Surace & Sanders 2000) and as an H II (Kim & Sanders 1998), and IRAS 15250+3609 is classified as both H II and LINER (Kim et al. 1995; Baan et al. 1998). The other two galaxies, IRAS 12112+0305 and IRAS 17208−0014, are classified as LINER (Veilleux et al. 1999) and H II (Kim et al. 1995), respectively. Our IFS data disagree with some of the previous classifications, in particular that of the two nuclei of IRAS 08572+3915 as H II (Arribas et al. 2000) and that of the true, optically hidden nucleus of IRAS 17208−0014 as a LINER (Arribas & Colina 2003).

2.2. *Observations*

Data were obtained with the INTEGRAL system (Arribas et al. 1998) plus the Wide Field Fibre Optical Spectrograph (WYFFOS; Bingham et al. 1994) in the 4.2 m William Herschel Telescope (WHT) at the Observatorio del Roque de los Muchachos (Canary Islands). Spectra were taken using the fiber bundle SB2 and a 600 line mm^{-1} grating with an effective resolution of ∼4.8 Å. Fibers in an INTEGRAL bundle are arranged in two sets: most of them (189 for SB2) form a rectangular area centered on the object, while the rest of them form a circle around it and simultaneously observe the sky. In the case of SB2, the covered field is $16\farcs5 \times 12\farcs3$. Data were taken under photometric conditions, and the seeing was ∼1″.0–1″.5 except for the 1998 April 1 observing run, when it was about 2″.0. Table 2 summarizes the parameters of the observations. In addition, *HST* imaging in the *I* band (Wide Field Planetary Camera 2 [WFPC2] F814W filter) is available for all of them and, with the exception of IRAS 15206+3342, also in the *H* band (Near-Infrared Camera and Multi-Object Spectrometer [NICMOS] F160W filter).

TABLE 2
Integral Field Observations

Galaxy	R.A. (J2000.0)	Decl. (J2000.0)	Spectral Range (Å)	t_{exp} (s)	Air Mass	P.A. (deg)	Date
IRAS 08572+3915	09 00 25.4	+39 03 54.1	5200–8100	1800 × 6	1.093	0.0	1998 Apr 01
IRAS 12112+0305	12 13 46.0	+02 48 41.0	4900–7900	1800 × 5	1.178	0.0	1998 Apr 02
	12 13 46.3	+02 48 29.7	5100–8100	1500 × 4	1.143	180.0	2001 Apr 14
IRAS 14348−1447	14 37 38.4	−15 00 22.8	5200–8200	1800 × 4	1.438	0.0	1998 Apr 01
IRAS 15206+3342	15 22 38.0	+33 31 36.6	5000–8100	1800 × 4	1.095	0.0	1998 Apr 03
IRAS 15250+3609	15 26 59.4	+35 58 37.6	4900–7900	1800 × 5	1.031	0.0	1998 Apr 02
IRAS 17208−0014	17 23 22.0	−00 17 00.1	5000–8100	1800 × 4	1.243	180.0	1998 Apr 03

Note.—Units of right ascension are hours, minutes, and seconds, and units of declination are degrees, arcminutes, and arcseconds.

3. DATA REDUCTION AND ANALYSIS

The basic reduction process includes bias subtraction, scattered light removal, extraction of the apertures, wavelength calibration, throughput and flat-field correction, sky subtraction, cosmic-ray rejection, and relative flux calibration. Although it is not strictly necessary for the present paper, an absolute flux calibration was also performed (Monreal-Ibero 2004).

For the present analysis, the strongest optical emission lines, including [O I] λ6300, Hα, [N II] $\lambda\lambda$6548, 6584, and [S II] $\lambda\lambda$6717, 6730, have been used. Each emission-line profile was fitted to a single Gaussian function using the DIPSO package inside the STARLINK environment.[4] The set of lines Hα + [N II] $\lambda\lambda$6548, 6584 was fitted simultaneously, fixing the separation in wavelengths between the three lines, assuming that all lines had the same width and fixing the ratio between the nitrogen lines at 3. Sulfur lines were fitted by fixing the distance between them and assuming the same width for both lines. In all cases, a constant value was assigned to the local continuum. A single (Gaussian) component is in general a good representation of the observed line profiles, with the exception of some nuclear regions. For these regions a two-component fit was necessary. The ionized gas velocity dispersion was derived from the Hα line width (after subtracting the instrumental profile in quadrature).

To study the ionization state, the line ratios [O I] λ6300/Hα, [N II] λ6584/Hα, and [S II] $\lambda\lambda$6717, 6731/Hα were calculated for each spectrum. Since the Hβ emission line was detected in an area substantially smaller than for the Hα line, these line ratios were not corrected for extinction. For the [N II] λ6584/Hα ratio, the two lines involved are so close to one another that reddening is negligible. In the case of the [S II] $\lambda\lambda$6717, 6731/Hα ratio, if extinction is moderate, the value of the ratio may change slightly, while in the regions where it is more elevated [$E(B-V) \gtrsim 1.0$], the extinction produces somewhat smaller ratios (typically by $\lesssim$0.1 dex). However, this small difference does not change the main conclusions of the present analysis. To better visualize the spatial distribution of the relevant magnitudes (e.g., Hα flux, velocity dispersion, and [N II] λ6584/Hα), two-dimensional images (maps) were created using a Renka & Cline two-dimensional interpolation method (Fig. 1). All these images have 81×81 pixels, with a scale of $0\farcs21$ pixel^{-1}.

4. RESULTS AND DISCUSSION

The kinematical properties of the galaxies under analysis have already been studied by Colina et al. (2005), who conclude that the global motions of the gas (i.e., velocity fields) are dominated by merger-induced flows, showing peak-to-peak velocity differences of $\sim$400 km s^{-1}. Only one of our six systems (IRAS 17208−0014) shows clear evidence of ordered rotational motions, although there are also some hints of rotation in IRAS 08572+3915. The ionized gas velocity dispersion maps revealed high-velocity regions ($\sim$70–200 km s^{-1}) that do not trace any special mass concentration. In the following subsections, we discuss the results derived from Figure 1, and in particular those from the Hα and velocity dispersion maps.

4.1. *Two-dimensional Ionization Structure of the Extranuclear Emission-line Nebulae*

Typical values of [O III] λ5007/Hβ in the brightest regions of these galaxies are around 1–2.5. Assuming similar values for fainter regions (where this ratio cannot be obtained due to the faintness of the lines), the [N II] λ6584/Hα ratio can be used to distinguish between LINER and H II–like ionization (see the diagnostic diagrams of Veilleux & Osterbrock 1987).

In general, the [N II] λ6584/Hα maps (see Fig. 1) show a complex ionization structure. According to this ratio, LINER-like emission is found in the extended extranuclear regions in three systems: IRAS 14348−1447, IRAS 15250+3609, and IRAS 17208−0014. By contrast, for IRAS 08572+3915, IRAS 15206+3342, and IRAS 12112+0305, this line ratio suggests a dominant H II–like ionization.

Similarly, the [S II] $\lambda\lambda$6717, 6731/Hα and the [O I] λ6300/Hα ratios have also been obtained, although in smaller fields due to a poorer signal. (The maps are not shown, but individual values are presented in Figs. 2 and 4.) As discussed by Dopita & Sutherland (1995), these line ratios, especially [O I] λ6300/Hα, are more reliable in distinguishing between H II– and LINER-like ionization. It is interesting to note that in general these line ratios indicate an ionization state higher than that inferred from the [N II] λ6584/Hα ratio. This is shown in Figure 2, which shows the [N II] λ6584/Hα versus [S II] $\lambda\lambda$6717, 6731/Hα for all the individual spectra/regions of the six systems of the sample. ([S II]/Hα instead of [O I]/Hα has been selected for this plot, since it covers a larger two-dimensional region.) In this figure, vertical and horizontal lines represent the frontier between the H II and LINER types of ionization. Many more spectra are classified as LINER according to the [S II] $\lambda\lambda$6717, 6731/Hα ratio (i.e., points located to the right of the vertical line) than according to [N II] λ6584/Hα (i.e., points above the horizontal line). In addition, most of the data points are located either in the LINER-like region according to both line ratios (i.e., top right quadrant) or in the region where the [S II] $\lambda\lambda$6717, 6731/Hα ratio is typical of LINERs but [N II] λ6584/Hα is typical of H II regions (i.e., bottom right quadrant).

For the sake of the following discussion, we define circumnuclear regions as those confined within the central $\sim$3″ (i.e., $r < 1\farcs5$, which is covered by $\sim$6 fibers/spectra) and extranuclear regions as those that typically extend for several kiloparsecs outward from this region (i.e., $r > 1\farcs5$). In Figure 2 we represent the circumnuclear and extranuclear regions with filled and open symbols, respectively. Note that the circumnuclear region corresponds roughly to the areas studied previously via long-slit spectroscopy. The circumnuclear data in this plot seem to be distributed in a more compact region, whereas the extranuclear data cover in general a wider range of these line quotients.

In order to investigate the different ionization alternatives, the line ratios predicted by different mechanisms are shown in Figure 2. Based in the apparent continuity between LINER and Seyfert spectra, along with the discovery of X-ray emission and the existence of a wide component in the Hα emission line of some LINERs, photoionization by a power-law spectrum coming from an AGN has been proposed as a possible ionizing mechanism (e.g., Ho et al. 1993; Groves et al. 2004). Although some of these models could in principle explain the line ratios measured in the circumnuclear regions, none of the nuclei of the sample are clearly located in the region identified by these models (see Fig. 2, where we have shown one of the models of as an example).

In general, the circumnuclear data show either H II–like spectra (indicative of intense star formation) or spectra of compound nature (LINER + H II). This agrees with the classification in the mid-infrared for these objects (Taniguchi et al. 1999; Rigopoulou et al. 1999) that includes them in the *starburst* group using the line-to-continuum ratio of polycyclic aromatic hydrocarbon (PAH) at 7.7 μm.

Regarding the extranuclear regions, the AGN models (Ho et al. 1993; Groves et al. 2004) are not, in general, likely to be

[4] See http://www.starlink.rl.ac.uk/.

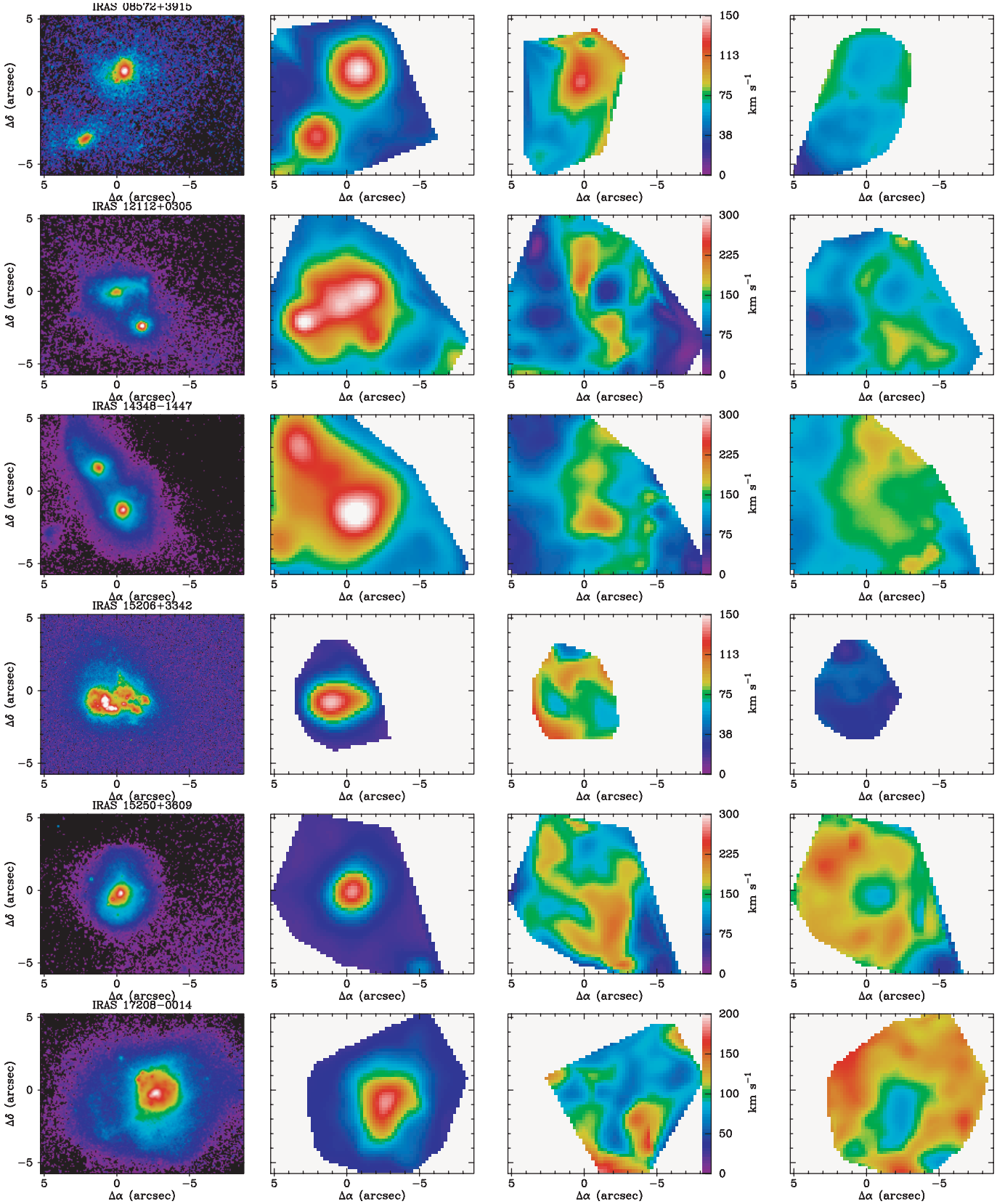

FIG. 1.—INTEGRAL maps for the main observables needed in the present paper. The distribution of the ionized gas is traced by the Hα emission line (*second column*), while the ionization state is traced by the [N II] λ6584/Hα ratio (*fourth column*). The color scale for this ratio has been chosen in a way that for a typical [O III] λ5007/Hβ ratio (i.e., $\sim$1.6; see the corresponding diagnostic diagrams of Veilleux & Osterbrock 1987), the limit between a LINER-like and a H II–like ionization is indicated by the green color (i.e., LINER-like excitation appears in red and yellow, while H II–like appears in blue). In addition, velocity dispersion maps are shown (*third column*). The high-resolution *HST H*-band images (*I* band for IRAS 15206+3342) appear in the first column as a tracer of the stellar distribution and for reference. North is up and east is left.

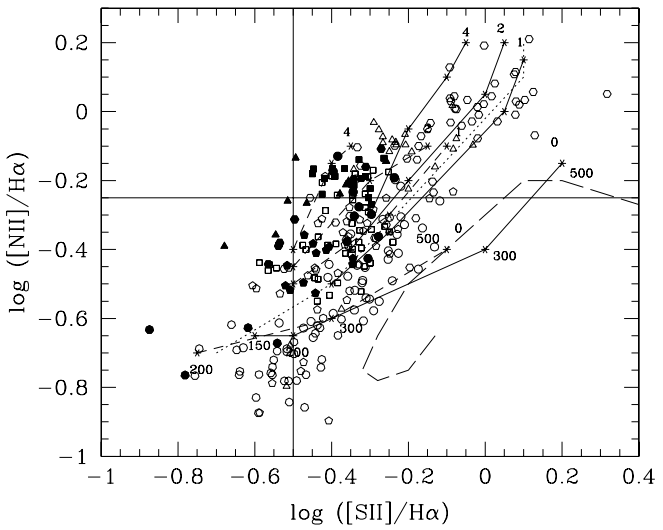

FIG. 2.—[N II] λ6584/Hα vs. [S II] $\lambda\lambda$6717, 6731/Hα ratios. This figure can be divided into several regions. In the bottom left corner is located the region occupied by typical H II regions, while the top right corner of the plot is the locus for a typical LINER-like spectrum. The symbol code used is the following: *pentagons*, IRAS 08572+3915; circles, IRAS 12112+0305; squares, IRAS 14348−1447; *heptagons*, IRAS 15206+3342; *triangles*, IRAS 15250+3609; *heptagons*, IRAS 17208−0014. Values for the fibers associated with the circumnuclear region are indicated with filled symbols, while those for the other fibers appear with open symbols. Models of Dopita & Sutherland (1995) for shocks have been superposed. Those without precursors are indicated with solid lines, while those with precursors are plotted using dashed lines. At the beginning of each line is shown the magnetic parameter $B/n^{1/2}$ (μG cm$^{3/2}$). Shock velocities range from 150 to 500 km s^{-1} for models without precursors and from 200 to 500 km s^{-1} for models with precursors. The long-dashed line indicates the [N II] λ6584/Hα and [S II] $\lambda\lambda$6717, 6731/Hα values predicted for photoionization by a power-law model for a dusty cloud at $n_e = 10^3$ cm^{-3} and $Z = Z_\odot$ (Groves et al. 2004). The dotted line indicates the locus for an instantaneous burst model of 4 Myr, $Z = Z_\odot$, IMF power-law slope of −2.35, and $M_{up} = 100\ M_\odot$; dust effects have been included, and $n_e = 10^3$ cm^{-3} (Barth & Shields 2000). [*See the electronic edition of the Journal for a color version of this figure.*]

representative of these low-density ($n_e < 10^3$ cm^{-3}) regions, as is also indicated by the relatively small fraction of data points located within the area defined by these models. However, it is interesting to note that the case of IRAS 17206−0014 may represent an exception in this context (see discussion in § 4.2). In short, although we cannot discard a possible contribution of AGN-like ionization in some regions, clearly this mechanism cannot explain in general the observed line ratios represented in Figure 2.

Ionization by young stars could be an obvious alternative mechanism to explain the line ratios. Barth & Shields (2000) have shown that starburst models during the Wolf-Rayet (WR)–dominated phase can explain the spectra of some LINERs, but only under very restricted conditions. In Figure 2 we have plotted the model of Barth & Shields that best fits the locus of our data as a dotted line. This corresponds to an instantaneous burst model of 4 Myr, $Z = Z_\odot$, initial mass function (IMF) power-law slope of −2.35, and $M_{up} = 100\ M_\odot$ and an interstellar medium characterized by an electron density (n_e) of 10^3 cm^{-3}. These conditions are very unlikely to be representative of the extranuclear regions of all these ULIRGs, especially taking into account the relatively young and short-lived population involved. (That is, for clusters younger than 3 Myr or older than 6 Myr, and for models with a constant star formation rate, the softer ionizing continuum results in an emission spectrum more typical of H II regions.) Furthermore, the fraction of ULIRGs with hints of WR signatures in their spectrum (i.e., broad optical feature at 4660 Å) is less than 10% (Armus et al. 1989).

The most likely mechanism to explain the observed ionization in the extended, extranuclear regions is the presence of large-scale shocks. Figure 2 presents the predicted line ratios for a representative set of shock models (Dopita & Sutherland 1995). These ratios agree with the range of observed values for shock velocities of 150–500 km s^{-1} in either a neutral (*solid lines*) or a preionized medium (*dashed lines*). Moreover, such high-speed flows are routinely detected in the extranuclear regions of ULIRGs as shown by detailed two-dimensional kinematic studies (Colina et al. 2005). Velocity fields inconsistent in general with ordered motions and with typical peak-to-peak velocities of 200–400 km s^{-1} are detected in the tidal tails and extranuclear regions of ULIRGs on scales of few to several kiloparsecs away from the nucleus and almost independent of the dynamical phase of the merger (see Colina et al. 2004, 2005 and references therein). Moreover, the presence of highly turbulent gas, as identified by large velocity dispersions of 70–200 km s^{-1} (Colina et al. 2005), further supports the scenario of fast shocks as the main ionization mechanism in these regions. In summary, the ionization of the extranuclear regions in the ULIRGs studied here can hardly be explained by accretion-powered AGNs or by young starbursts but is consistent with fast, large-scale shocks.

4.2. *Excitation and Velocity Dispersions: Further Evidence for Ionization by Shocks*

The positive correlation between the velocity dispersion and ionization found by some authors using circumnuclear (slit) spectra of ULIRGs has been considered as further evidence supporting the presence of shocks in these objects (Armus et al. 1989; Dopita & Sutherland 1995; Veilleux et al. 1995). The present study also supports the correlation previously observed. As shown in Figure 3, the [S II] $\lambda\lambda$6717, 6731/Hα and velocity dispersion values derived from the integrated spectra, i.e., combining the individual spectra for each object, are consistent with previous results (Armus et al. 1989). However, these spectra are not necessarily representative of the extranuclear regions.

In Figure 4 we present similar plots, but now each data point represents the value for a specific spectrum (fiber, i.e., different position in the extranuclear nebula) but excluding the circumnuclear region, for each individual galaxy, and using three different

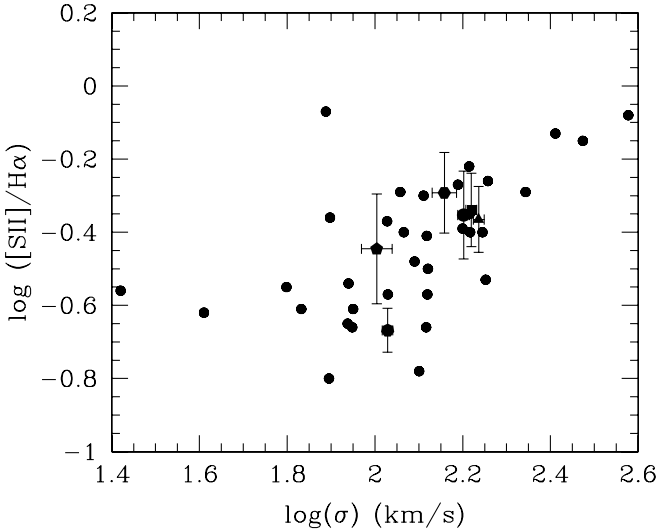

FIG. 3.—Line width–line intensity correlation for LIRGs. Our data are plotted with error bars, while the other points are taken from Armus et al. (1989). Symbols are the same as in Fig. 2. Error bars were derived from the errors in the line fitting. [*See the electronic edition of the Journal for a color version of this figure.*]

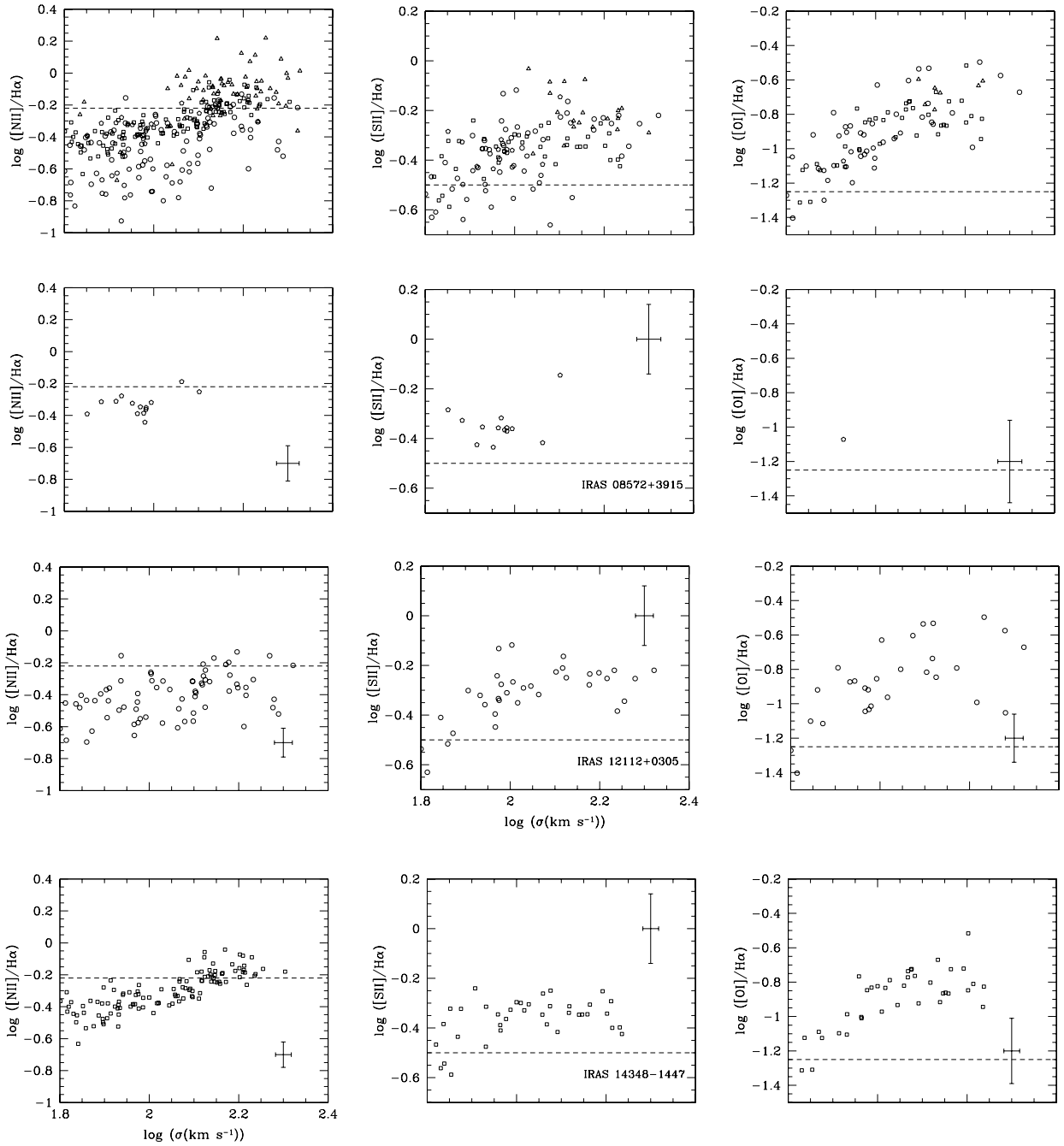

FIG. 4.—Relation between the velocity dispersion and [N II] λ6584/Hα (*left*), [S II] λλ6717, 6731/Hα (*middle*), and [O I] λ6300/Hα (*right*). The dashed horizontal line marks the frontiers between the H II region and LINER-type ionization. The top row shows the combined data for all the systems with the exception of IRAS 17206−0014. The following rows show data for the individual systems. The mean errors for each galaxy are shown in the corners of the plots. Symbols are the same as in Fig. 2. [*See the electronic edition of the Journal for a color version of this figure.*]

line ratios ([N II] λ6584/Hα, [S II] λλ6717, 6731/Hα, and [O I] λ6300/Hα). The dashed horizontal lines indicate the borderline between H II and LINER ionization. In the top panels the data for the individual galaxies (except IRAS 17208−0014; see below) are combined. These panels indicate that while the correlation of the velocity dispersions with the line ratio is not so well defined for [N II] λ6584/Hα, for the other two line ratios, and especially for [O I] λ6300/Hα (i.e., the most reliable diagnostic ratio to detect ionization by shocks according to models by Dopita & Sutherland 1995), the correlation is clear. The fact that the extranuclear data of these five systems follow a well-defined relation between the line ratio and the velocity dispersion reinforces the idea that shocks are also the dominant ionization source at large scales (>2–3 kpc). Individually, two systems, IRAS 12112+0305 and IRAS 14348−1447, show a clear correlation in the three line ratios. For three of the remaining systems, IRAS 08572+3915, IRAS 15206+3342, and IRAS 15250+3609, the range in velocity dispersion is too small to show the correlation.

Finally, IRAS 17208−0014 does not follow the mean behavior observed in the other systems, showing a wider range of line ratio values. This galaxy has been studied in detail by Arribas & Colina (2003) and Colina et al. (2005), and it is the only clear case in this sample showing rotation on scales of several kiloparsecs. This may be an indication that this system is in a different (probably more evolved) dynamical phase and/or that it has had a different merging history. In any event, the fact that the gas

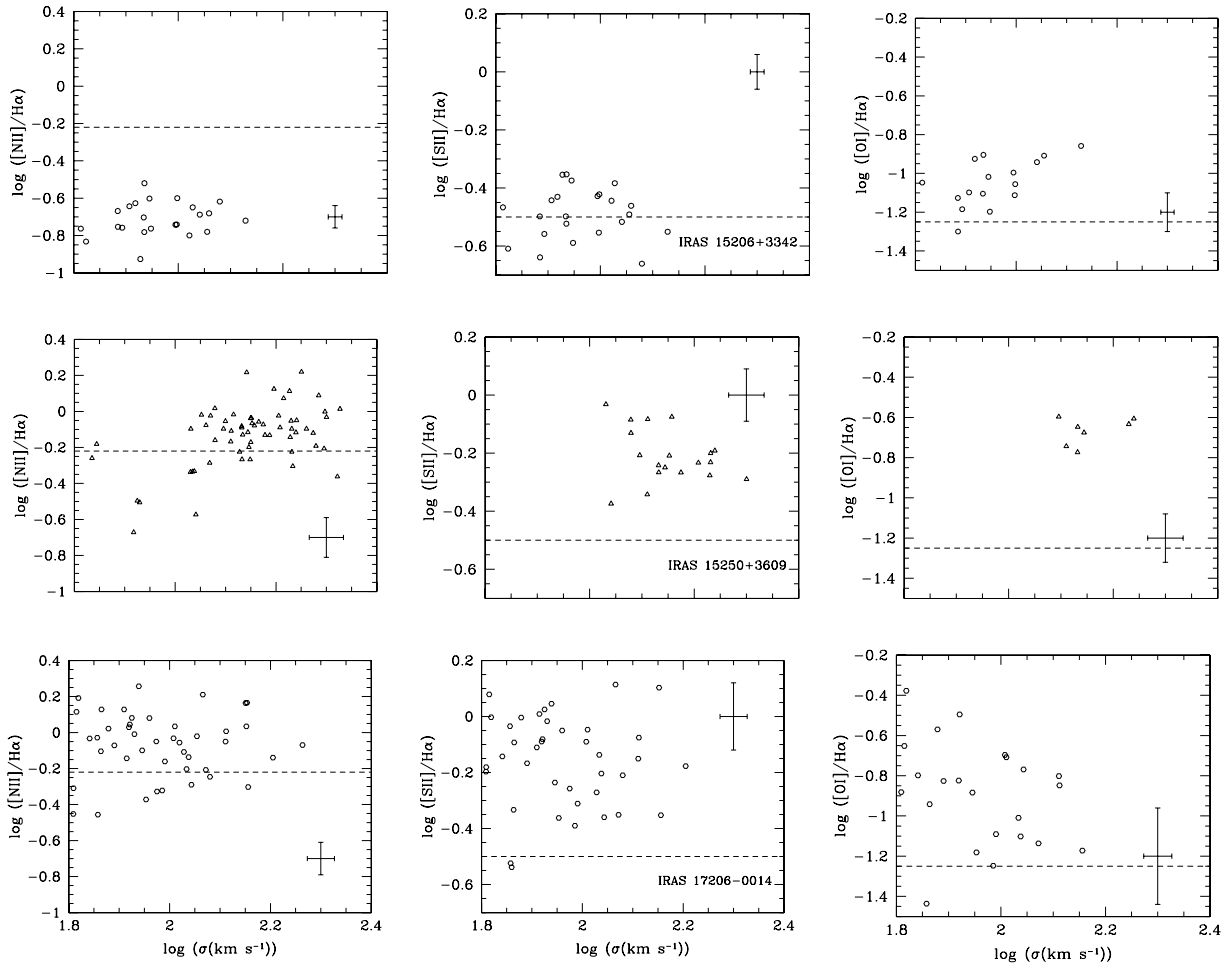

FIG. 4.—*Continued*

kinematics indicates a more relaxed and virialized system suggests that shocks are not the dominant ionization mechanism in this galaxy, and therefore the above-mentioned correlation should not be expected. For this galaxy the origin of the LINER-like ionization in the extranuclear region should be different (note that the three line ratios shown in Fig. 4 are consistent with LINER-like ionization). A hint that this is the case comes from the detection of an extended ($\sim$4 kpc) hard X-ray nebula in this galaxy (Ptak et al. 2003), which would provide an ionizing spectrum similar to that of an AGN. This may explain the fact that the excitation of this object is higher than that of the rest of the galaxies and similar to that expected from a low-luminosity AGN (Fig. 2; Ho et al. 1993).

4.3. *Origin of the Shocks in the Circumnuclear and Extranuclear Regions: Superwinds and Merger-Induced Flows*

In previous sections, shocks have been identified as the main ionization mechanism in the extended, extranuclear ionized regions. Moreover, the detection of a positive correlation between the ionization status of the gas, as best indicated by the shock tracer [O I] λ6300/Hα ratio, and the velocity dispersion of the gas suggests a direct causal relation between the LINER ionization and the presence of shocks. What is the origin of the shocks in the circumnuclear region and in the extranuclear regions extended at distances of up to 10–15 kpc from the nucleus? Some authors have found evidence supporting the existence of so-called superwinds generated by the combined effect of massive stars' winds and supernova explosions in intense nuclear starbursts (Heckman et al. 1990). These superwinds, identified by the presence of kinematically distinct components in the profiles of the emission (Heckman et al. 1990) or absorption lines (Martin 2005; Rupke et al. 2005a, 2005b), generate shocks in the circumnuclear regions as the stellar winds move through the interstellar medium.

Recent studies in a large sample of LIRGs and ULIRGs conclude that the presence of superwinds has to be an almost universal phenomenon in the circumnuclear regions of ULIRGs (typical angular sizes of about 1″ or 1–2 kpc, depending on redshift), as kinematically distinct components of the neutral interstellar NaD lines, blueshifted by a median velocity of 350 km s^{-1}, are detected in at least 70% of ULIRGs (Martin 2005; Rupke et al. 2005a, 2005b). These velocity components are also detected in our integral field spectra for some systems. Of the six galaxies in the sample, our data show the presence of double Hα line profiles in the circumnuclear regions of the northern and southern nuclei of the interacting pairs IRAS 12112+0305 and IRAS 14347−1448 (see Fig. 5). These secondary velocity components are blueshifted with respect to the system by 150 and 300 km s^{-1}, respectively. In addition to these galaxies, similar signatures have been identified in the circumnuclear regions of more evolved ULIRGs such as IRAS 15250+3609 ($V - V_{\rm sys} = -170$ km s^{-1}; Monreal-Ibero 2004) and Arp 220 (peak-to-peak velocity of 1000 km s^{-1}; Arribas et al. 2001). However, our IFS data show that the presence of double components, when detected, is always confined to the nuclear and circumnuclear regions, i.e., distances

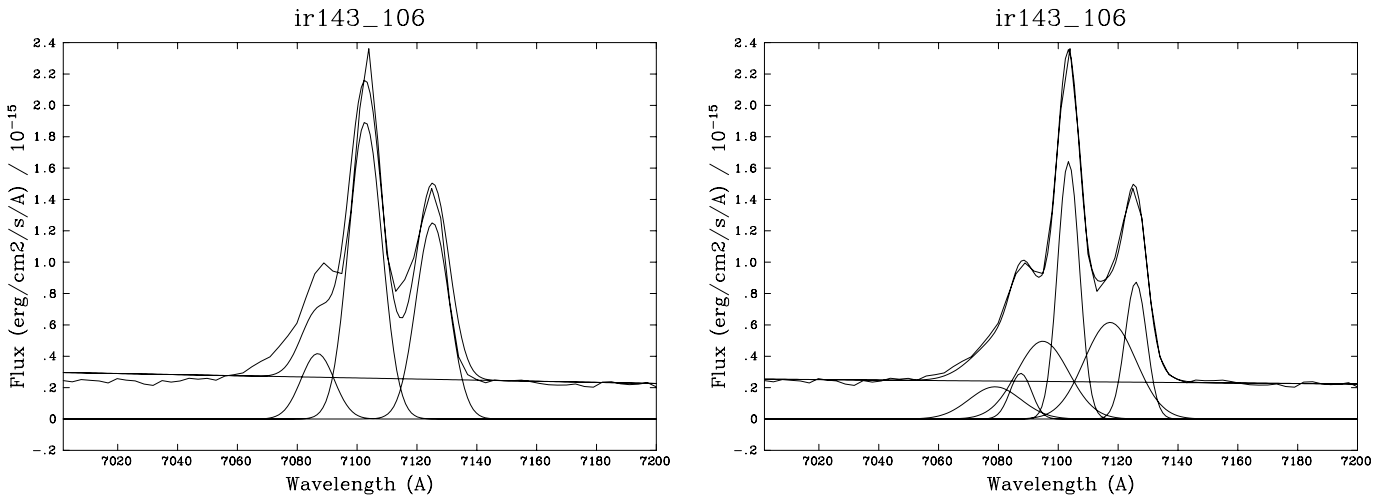

FIG. 5.—Fitting of Hα + [N II] $\lambda\lambda$6548, 6584 lines in IRAS 14348−1447 to one or two sets of Gaussian functions for fiber 106.

of 1–2 kpc from the nucleus. The lack of detection of double components in the extranuclear regions, at distances of several kiloparsecs away from the nucleus, can be interpreted as though the high-velocity outflows associated with the nuclear superwinds were not present at these distances or as though they were of much lower amplitude (less than 100 km s^{-1}), and therefore they have not been detected as kinematically distinct components with the present spectral resolution.

On the other hand, the complex two-dimensional velocity field and velocity dispersion structure of the extranuclear ionized regions of ULIRGs (Colina et al. 2004, 2005) shows in general large velocity gradients with peak-to-peak velocities of a few to several hundreds of kilometers per second associated with tidal tails and extranuclear regions at distances of several kiloparsecs away from the massive circumnuclear starbursts. Moreover, the largest values of the velocity dispersion in many ULIRGs (up to 200 km s^{-1}) are detected not in the nucleus but in extranuclear regions (Colina et al. 2005), implying therefore the presence of an extended, highly turbulent medium on kiloparsec size scales. As shown by specific models of the nearest ULIRG, Arp 220, tidally induced flows lead to relative gas velocities that are much larger than the original impact velocities of the galaxies (McDowell et al. 2003), and therefore high-speed flows of several hundreds of kilometers per second are a natural consequence of the merging process associated with ULIRGs. The presence of these tidally induced, high-velocity flows and highly turbulent medium will generate shocks that in turn will heat and ionize the interstellar medium, producing the observed LINER-type spectra as in the nearest ULIRG, Arp 220 (McDowell et al. 2003; Colina et al. 2004). In short, the lack of superwind signatures and the kinematic properties of the gas in the extranuclear regions supports the idea that merger-induced flows are the origin of the fast shocks producing the LINER-like excitation in these extended regions.

5. CONCLUSIONS

Integral field spectroscopy with the INTEGRAL fiber system has been used to analyze the circumnuclear and extranuclear ionization structure of six low-z ULIRGs. The main results can be summarized as follows:

1. The two-dimensional ionization characteristics of the extranuclear regions of these galaxies correspond to those of LINERs. This is clearly indicated by the [S II] $\lambda\lambda$6717, 6731/Hα and especially the [O I] λ6300/Hα line ratios, which allow us to discriminate reliably between the H II and LINER ionization in low-excitation conditions (i.e., [O III] λ5007/H$\beta \leq 2.5$).

2. The observed LINER-type line ratios in the extranuclear regions are in general better explained with ionization by fast shocks with velocities of 150–500 km s^{-1} rather than with AGN or starburst photoionization. Further evidence pointing to shocks as the dominant source of ionization comes from a positive correlation between the ionization state and the velocity dispersion of the ionized gas. The present two-dimensional data show that this correlation holds especially if the [O I] λ6300/Hα line ratio is used.

3. Although signatures for superwinds are observed in the circumnuclear regions of some systems, no kinematic evidence for such a mechanism is found in the extranuclear regions. Alternatively, the shocks that produce the observed LINER-type ionization in the extranuclear regions could be due to a different phenomenon. Taking into account the general two-dimensional kinematic characteristics of the extranuclear regions in these objects, which indicate disordered motions with peak-to-peak velocities of about 400 km s^{-1} and velocity dispersions of up to 200 km s^{-1}, the origin of the shocks is most likely tidally induced large-scale flows produced during the merging process.

4. The galaxy IRAS 17208−0014 presents a peculiar kinematical and ionization structure. For this galaxy, the origin of the LINER-type ionization in the extranuclear region is most likely explained by the presence of the recently detected hard X-ray extended (4 kpc) emission that would produce an ionizing spectrum similar to that of an AGN. This may explain the fact that the excitation of this object is higher than that of the rest of the galaxies and compatible with that expected in low-luminosity AGNs.

A. M.-I. acknowledges support from the Euro3D Research Training Network, funded by the EC (HPRN-CT-2002-00305). Financial support was provided by the Spanish Ministry for Education and Science through grant AYA2002-01055. This work is based on observations with the William Herschel Telescope operated on the island of La Palma by the ING in the Spanish Observatorio del Roque de los Muchachos of the Instituto de Astrofísica de Canarias.

REFERENCES

Armus, L., Heckman, T. M., & Miley, G. K. 1989, ApJ, 347, 727
Arribas, S., & Colina, L. 2003, ApJ, 591, 791
Arribas, S., Colina, L., & Borne, K. D. 2000, ApJ, 545, 228
Arribas, S., Colina, L., & Clements, D. 2001, ApJ, 560, 160
Arribas, S., et al. 1998, Proc. SPIE, 3355, 821
Baan, W. A., Salzer, J. J., & Lewinter, R. D. 1998, ApJ, 509, 633
Barth, A. J., & Shields, J. C. 2000, PASP, 112, 753
Bingham, R. G., Gellatly, D. W., Jenkins, C. R., & Worswick, S. P. 1994, Proc. SPIE, 2198, 56
Borne, K. D., Bushouse, H., Lucas, R. A., & Colina, L. 2000, ApJ, 529, L77
Clements, D. L., Sutherland, W. J., McMahon, R. G., & Saunders, W. 1996, MNRAS, 279, 477
Colina, L., Arribas, S., Borne, K. D., & Monreal, A. 2000, ApJ, 533, L9
Colina, L., Arribas, S., & Clements, D. 2004, ApJ, 602, 181
Colina, L., Arribas, S., & Monreal-Ibero, A. 2005, ApJ, 621, 725
Dopita, M. A., & Sutherland, R. S. 1995, ApJ, 455, 468
Frayer, D. T., Armus, L., Scoville, N. Z., Blain, A. W., Reddy, N. A., Ivison, R. J., & Smail, I. 2003, AJ, 126, 73
Genzel, R., & Cesarsky, C. J. 2000, ARA&A, 38, 761
Genzel, R., Tacconi, L. J., Rigopoulou, D., Lutz, D., & Tecza, M. 2001, ApJ, 563, 527
Groves, B. A., Dopita, M. A., & Sutherland, R. S. 2004, ApJS, 153, 9
Heckman, T. M., Armus, L., & Miley, G. K. 1990, ApJS, 74, 833
Heckman, T. M., Lehnert, M. D., Strickland, D. K., & Armus, L. 2000, ApJS, 129, 493
Ho, L. C., Filippenko, A. V., & Sargent, W. L. W. 1993, ApJ, 417, 63
Kim, D.-C., & Sanders, D. B. 1998, ApJS, 119, 41
Kim, D.-C., Sanders, D. B., Veilleux, S., Mazzarella, J. M., & Soifer, B. T. 1995, ApJS, 98, 129
Le Floc'h, E., et al. 2004, ApJS, 154, 170
Lehnert, M. D., & Heckman, T. M. 1996, ApJ, 462, 651
Martin, C. L. 2005, ApJ, 621, 227
McDowell, J. C., et al. 2003, ApJ, 591, 154
Monreal-Ibero, A. 2004, Ph.D. thesis, Univ. La Laguna
Ptak, A., Heckman, T., Levenson, N. A., Weaver, K., & Strickland, D. 2003, ApJ, 592, 782
Rigopoulou, D., Spoon, H. W. W., Genzel, R., Lutz, D., Moorwood, A. F. M., & Tran, Q. D. 1999, AJ, 118, 2625
Rupke, D. S., Veilleux, S., & Sanders, D. B. 2002, ApJ, 570, 588
———. 2005a, ApJS, 160, 87
———. 2005b, ApJS, 160, 115
Sanders, D. B., & Mirabel, I. F. 1996, ARA&A, 34, 749
Sanders, D. B., Soifer, B. T., Elias, J. H., Madore, B. F., Matthews, K., Neugebauer, G., & Scoville, N. Z. 1988, ApJ, 325, 74
Scoville, N. Z., et al. 2000, AJ, 119, 991
Surace, J. A., & Sanders, D. B. 2000, AJ, 120, 604
Surace, J. A., Sanders, D. B., & Evans, A. S. 2000, ApJ, 529, 170
Tacconi, L. J., Genzel, R., Lutz, D., Rigopoulou, D., Baker, A. J., Iserlohe, C., & Tecza, M. 2002, ApJ, 580, 73
Taniguchi, Y., Yoshino, A., Ohyama, Y., & Nishiura, S. 1999, ApJ, 514, 660
Veilleux, S., Cecil, G., & Bland-Hawthorn, J. 2005, ARA&A, 43, 769
Veilleux, S., Kim, D.-C., & Sanders, D. B. 1999, ApJ, 522, 113
Veilleux, S., Kim, D.-C., Sanders, D. B., Mazzarella, J. M., & Soifer, B. T. 1995, ApJS, 98, 171
Veilleux, S., & Osterbrock, D. E. 1987, ApJS, 63, 295